^{6}He interaction with protons

K. Rusek*
Department of Nuclear Reactions, The Andrzej Sołtan Institute for Nuclear Studies, Hoża 69, PL-00-681 Warsaw, Poland

K. W. Kemper
Physics Department, Florida State University, Tallahassee, Florida 32306-4350

R. Wolski
Department of Nuclear Reactions, The Henryk Niewodniczański Institute of Nuclear Physics, Radzikowskiego 152, PL-31-342 Cracow, Poland
and Flerov Laboratory of Nuclear Reactions, Joint Institute for Nuclear Research, RU-141980 Dubna, Russia
(Received 14 June 2000; revised manuscript received 19 March 2001; published 19 September 2001)

Experimental data for ^{6}He+^{1}H elastic scattering and the two-neutron transfer reaction, measured recently at the Joint Institute for Nuclear Research in Dubna, Russia, were analyzed by coupled channels calculations using a dineutron model of ^{6}He. The results of the analysis reveal that all the processes induced by ^{6}He on a hydrogen target are coupled. This analysis shows that the couplings to the $^6\mathrm{He}\rightarrow\alpha+2n$ breakup channels can be included in a simple optical model calculation by means of a polarization potential that is repulsive and whose strength is about 25% of the single-folding potential. Predictions for the $p+^6$He inelastic scattering to the 2^+ resonance are made. A good description of the two-neutron transfer reaction data is obtained when the triton transfer process is coherently added to the dineutron transfer. The spectroscopic amplitude of the $t+t$ component of the ^{6}He ground-state wave function is found to have the opposite sign to that of $\alpha+2n$ with a magnitude close to that predicted by a microscopic four-cluster model of ^{6}He.

DOI: 10.1103/PhysRevC.64.0346XX PACS number(s): 24.10.Eq, 25.70.Bc

I. INTRODUCTION

The cluster structure of the nucleus ^{6}He has recently been investigated in a series of experiments with radioactive ^{6}He beams scattered from ^{4}He and ^{1}H targets [1,2]. The main purpose of those experiments, performed at the Joint Institute for Nuclear Research in Dubna, Russia, was to establish the dineutron and cigarlike $\alpha+2n$ configurations predicted for the ^{6}He ground-state wave function by microscopic three-body calculations [3]. The two-neutron transfer reaction data were analyzed by distorted wave Born approximation (DWBA) calculations [1,2,4,5]. The results strongly suggest that the dineutron configuration dominates the ^{6}He ground state while the cigarlike component of the ^{6}He ground-state wave function contributes only negligibly to the differential cross section of the two-neutron transfer reaction. This observation is in agreement with predictions, as the cigarlike component of the ^{6}He ground-state wave function corresponds to a much smaller separation between the α core and the center of mass of the two valence neutrons than the dineutron component.

Apart from the $\alpha+2n$ configuration, the ground state of ^{6}He is known to have a well-defined $t+t$ cluster structure, which was experimentally investigated by means of $(t,^6\mathrm{He})$ transfer reactions on a number of targets by Clarke [6]. Theoretical calculations predict the spectroscopic factors for this configuration to range from 0.44 [7] up to 1.77 [6,8] depending on the model. In a very recent analysis of proton-induced reactions on ^{6}He below the three-body breakup threshold [9], a spectroscopic factor equal to 1.77 was used. DWBA analysis of the $^1\mathrm{H}(^6\mathrm{He},\alpha)^3\mathrm{H}$ reaction performed by Wolski *et al.* [2] led to the conclusion that this spectroscopic factor is much smaller. In a similar analysis of the same data set by Oganessian *et al.* [4,5] the experimental data were described without any *t*-transfer component. This result contradicts the theoretical predictions for $t+t$ clustering in $^6\mathrm{He}_{\mathrm{g.s.}}$.

Neutron-rich ^{6}He is a very weakly bound nucleus and can easily dissociate into an α particle and two neutrons in the field of the target nucleus. Coupling to the $^6\mathrm{He}\rightarrow\alpha+2n$ breakup states has been found to strongly affect the process of ^{6}He+^{4}He elastic scattering in a broad range of incident energies [10]. Similar effects of the breakup channels were also previously reported for other weakly bound projectiles like *d*, ^{6}Li or ^{9}Be. Thus, one may surmise that ^{6}He breakup can also play an important role in the ^{6}He+^{1}H interaction and have an influence on the two-neutron transfer reaction. Recently Gupta *et al.* [11] analyzed existing data for proton elastic scattering from ^{4,6,8}He and ^{6,7,9,11}Li in a wide energy range by optical model calculations with a central potential derived from nucleon-nucleon interactions. They found that the depth of the potential has to be significantly reduced for all the nuclei except ^{4}He, suggesting strong channel coupling effects for the other nuclei. In the DWBA analyses of the $^1\mathrm{H}(^6\mathrm{He},\alpha)^3\mathrm{H}$ reaction performed so far [2,4,5], the breakup effects of the projectile have not been explicitly included.

In this work we present a consistent analysis of existing ^{6}He+^{1}H elastic scattering and two-neutron transfer reaction data at an incident energy of 151 MeV [2] by coupled channels calculations, with breakup effects included. The aim of this work is to study the role of the couplings to the ^{6}He

*Electronic address: rusek@fuw.edu.pl

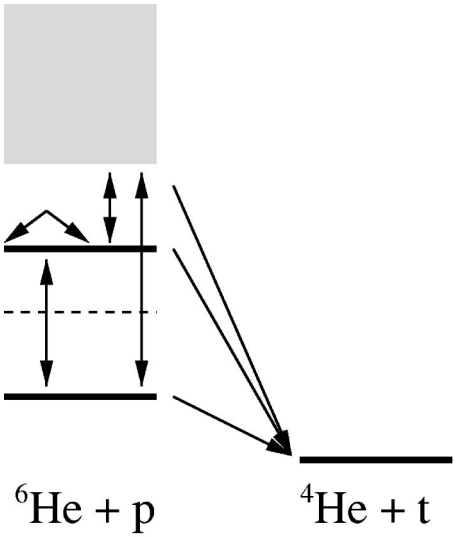

FIG. 1. Coupling scheme used in the analysis.

$\rightarrow \alpha + 2n$ breakup states and transfer of the dineutron from these states in the ^{6}He-proton interaction. The scheme of the couplings used in the analysis is shown in Fig. 1. The calculations were performed using the code FRESCO [12], in two-steps. First, elastic scattering data were analyzed by means of the coupled-discretized-continuum channels (CDCC) method [13]. In these calculations, described in Sec. II, the α + dineutron cluster model of ^{6}He was applied and couplings to the unbound states of ^{6}He were taken into account. Next, the two-neutron transfer reaction was included, allowing transfer of the dineutron cluster from the ground state and from the unbound states of ^{6}He (coupled channels Born approximation, CCBA). The triton transfer process, experimentally indistinguishable, was coherently added to the dineutron transfer. These calculations are described in Sec. III. The results of these calculations are summarized in Sec. IV.

II. ELASTIC AND INELASTIC SCATTERING

A. Dineutron model of ^{6}He

In this work, the nucleus ^{6}He was assumed to have a two-body $\alpha + 2n$ cluster structure with the spin of the dineutron $(2n)$ cluster set to $s=0$. The internal energy of the dineutron cluster was taken as zero. The calculations were performed with three different geometries (R_0, a_0) of the Woods-Saxon potential binding the two clusters. The parameters of the potential are listed in Table I as sets I, II, and III.

The wave function describing the relative motion of the two clusters in the ground state of ^{6}He, $\Psi_0(r)$, was calculated in the potential well with the depth V_0 varied to reproduce the binding energy of 0.975 MeV. The wave function of the 2^+ resonant state of ^{6}He at excitation energy of 1.80 MeV, $\Psi_2(r)$, was calculated using the CDCC method [10]. The energy bin of 0.3 MeV width, roughly corresponding to the empirical value, was set at the excitation energy of 0.825 MeV above the $^6\mathrm{He} \rightarrow \alpha + 2n$ breakup threshold. The cluster wave functions, $\phi(r,E)$, calculated within the bin were averaged over the bin width [Eq. (1)] and the wave function calculated this way was used as the wave function of the resonance. The depth of the binding potential was adjusted to give a resonance at the required excitation energy of 1.80 MeV.

The spectroscopic amplitudes for the ground state of ^{6}He and for the 2^+ resonance were calculated using the method presented in Refs. [14,15]. For both states the calculated values were very close to unity therefore in the present work the amplitudes were assumed to be equal to 1.0.

The three different geometries of the α-$2n$ binding potential used in the calculations generated three sets of wave functions for the ground state and the 2^+ resonance as well as different properties of ^{6}He such as rms radii and $B(E2;\mathrm{g.s.} \rightarrow 2^+)$ values. Set I was used in our previous analysis of $^6\mathrm{He}+^4\mathrm{He}$ elastic scattering [10] and corresponds to a large separation between the two clusters, rms $=4.92$ fm, and a large value of the reduced transition probability, $B(E2;\mathrm{g.s.} \rightarrow 2^+) = 7.08\ e^2\,\mathrm{fm}^4$. Set II was chosen so that the calculated value of the reduced transition probability, $3.21\ e^2\,\mathrm{fm}^4$, corresponds closely to the empirical value reported by Aumann *et al.* [16]. In this case the separation between the two clusters is much smaller, rms $=4.36$ fm. The last geometry, set III, gives the separation between the two clusters in ^{6}He equal to the separation between the α-d clusters in ^{6}Li, rms $=4.06$ fm [17]. For this geometry the

TABLE I. Parameters of the binding potentials and spectroscopic amplitudes. In the last two columns the quantum numbers, NL, and the signs of the wave functions at the particle-core separation $r=15$ fm are given.

	V_0 (MeV)	R_0 (fm)	a_0 (fm)	Ref.	S_a	Ref.	NL	sign of $\Psi(r)$
$^6\mathrm{He}_{\mathrm{g.s.}} = \alpha + 2n$, set I	69.363	1.90	0.65	[10]	1.0	[14,15]	$2S$	-
$^6\mathrm{He}_{exc.} = \alpha + 2n$, set I	80.427	1.90	0.65	[10]	1.0	[14,15]	$1D$	+
$^6\mathrm{He}_{\mathrm{g.s.}} = \alpha + 2n$, set II	84.520	1.90	0.39		1.0	[14,15]	$2S$	-
$^6\mathrm{He}_{exc.} = \alpha + 2n$, set II	90.796	1.90	0.39		1.0	[14,15]	$1D$	+
$^6\mathrm{He}_{\mathrm{g.s.}} = \alpha + 2n$, set III	93.512	1.90	0.25		1.0	[14,15]	$2S$	-
$^6\mathrm{He}_{exc.} = \alpha + 2n$, set III	91.517	1.90	0.25		1.0	[14,15]	$1D$	+
$^6\mathrm{He}_{\mathrm{g.s.}} = t + t$	102.728	1.90	0.65	[6,9]	-0.5	This work	$2S$	+
$^4\mathrm{He}_{\mathrm{g.s.}} = p + t$	61.032	2.00	0.40	[29]	1.4142	[8]	$1S$	+
$^3\mathrm{H}_{\mathrm{g.s.}} = p + 2n$	44.382	2.00	0.60	[29]	1.2247	[8]	$1S$	+

TABLE II. Parameters of the input optical model potentials.

	V_0 (MeV)	R_0 (fm)	a_0 (fm)	W_S (MeV)	W_D (MeV)	R_i (fm)	a_i (fm)	V_{LS} (MeV)	R_{LS} (fm)	a_{LS} (fm)	Ref.
$\alpha+{}^3$He, *A*	173.0	2.28	0.145	1.12	0.00	5.29	1.050	1.00	2.28	0.145	[30]
$\alpha+{}^3$He, *B*	142.92	2.57	0.271	0.86	0.00	6.88	0.972	0.00	0.00	0.000	
$\alpha+{}^3$He, *C*	78.57	1.80	0.700	10.00	0.00	1.80	0.70	0.00	0.00	0.000	[29]
$d+{}^1$H	65.8	1.25	0.501	0.00	10.0	1.20	0.517	0.00	0.00	0.000	
$p+{}^4$He	48.949	1.75	0.477	0.00	0.557	1.75	0.477	4.26	1.75	0.350	

calculated value of the reduced transition probability $B(E2;\text{g.s.}\rightarrow 2^+)=2.06\ e^2\ \text{fm}^4$, is the smallest.

The continuum above the $^6\text{He}\rightarrow\alpha+2n$ breakup threshold was discretized into momentum bins of equal widths, $\Delta k=0.25\ \text{fm}^{-1}$, as in our previous analysis of $^6\text{He}+^4\text{He}$ elastic scattering [10]. Here $\hbar k$ is the momentum of the α-dineutron relative motion. The wave functions $\Psi(r)$ representing those bins were calculated by means of the CDCC method,

$$\Psi(r)=\frac{1}{\sqrt{\Delta k}}\int_{\Delta k}\phi(r,k)dk. \tag{1}$$

For the bins corresponding to the angular momentum of the two clusters' relative motion $L=0$, 1, 3, the binding potential of the ^{6}He ground state was used, while for the $L=2$ bins the binding potential was the same as the one found for the 2^+ resonance.

B. Potentials

The central potential in the $^6\text{He}+^1\text{H}$ entrance channel as well as all the coupling potentials used in the calculations were derived from empirical p-^{4}He and d-^{1}H potentials by means of a single-folding method,

$$U^{SF}_{i\rightarrow f}(R)=\langle\Psi_f(r)|U_{p\text{-}d}(|\vec{R}+2/3\ \vec{r}|) + U_{p\text{-}\alpha}(|\vec{R}-1/3\ \vec{r}|)|\Psi_i(r)\rangle, \tag{2}$$

where R is the separation between the projectile and the target while r is the distance between the clusters in ^{6}He. The choice of these optical model potentials, $U_{p\text{-}d}$ and $U_{p\text{-}\alpha}$, determined the final results of the calculations, therefore the scattering of α particles and deuterons from protons was examined by us. Fortunately, there are experimental data for both scattering systems at energies very close to the required values of $E_d=\frac{2}{6}\ 151\ \text{MeV}=45.3\ \text{MeV}$ and of $E_\alpha=\frac{4}{6}\ 151\ \text{MeV}=100.7\ \text{MeV}$. We have used the data sets of Hinterberger *et al.* [18] for $d+^1$H elastic scattering at $E_d=52$ MeV and by Plummer *et al.* [19] for $p+^4$He elastic scattering at $E_p=26.1$ MeV.

The data of Plummer *et al.* were analyzed by means of optical model calculations. An automatic search was performed using the code ECIS79 [20]. Starting parameters for the search were taken from the study of Thompson *et al.* [21]. In the course of the calculations it was found that the exchange term due to the triton-transfer reaction plays an important role at scattering angles larger than 100°. Therefore, only forward angle scattering data were fitted. The final results of the search are listed in Table II.

Strong effects due to contributions from the transfer reaction were also found for the $d+^1$H elastic scattering at 52 MeV. Here these effects could be accounted for by a significant increase of the imaginary part of the optical potential found by Hinterberger *et al.* [18]. Good description of the experimental data was achieved with the potential parameters listed in Table II.

A severe test of the empirical optical model potentials used as input to the single-folding calculations could be an analysis of $^6\text{Li}+^1\text{H}$ elastic scattering at an energy close to 151 MeV. If the choice of the input potentials is correct, CDCC calculations for this scattering system should reproduce the experimental data. Since there exist experimental data for this scattering system, corresponding to the lithium laboratory energy of 155.4 MeV [22], such test calculations were performed. In the calculations a cluster $\alpha+d$ model of ^{6}Li, used by us previously [17], was adopted. All the parameters of the model including discretization and truncation of the continuum states as well as details of the CDCC method were discussed in Ref. [17] and are not repeated here.

The results of the calculations are compared to the experimental data for elastic scattering of ^{6}Li from protons at the energy of 155.4 MeV in Fig. 2. One-channel calculations without couplings to any excited states of ^{6}Li, with the central ^{6}Li-p potential generated from optical model potentials for $p+^4$He and $d+^1$H, are marked as 1ch $N_i=1.0$. The results of the calculations overestimate by far the experimental data. Better results were obtained when the couplings to the resonant excited states of ^{6}Li as well as to the continuum were included by means of the CDCC method. However, CDCC calculations still overestimate the experimental data. This result suggests that contributions from other processes not included in the coupling scheme are present. Limited computing capacity did not allow us to extend the coupling scheme for more breakup states or to the one-neutron transfer reaction. Therefore one *free* parameter was introduced into the calculations. The depth of the imaginary part of the input $d+^1$H potential was multiplied by a normalization factor N_i. When this factor was increased to 1.7, the experimental data were well reproduced up to a scattering angle of about 140° (dashed curve in Fig. 2). At the very backward angles the calculations did not reproduce the experimental data.

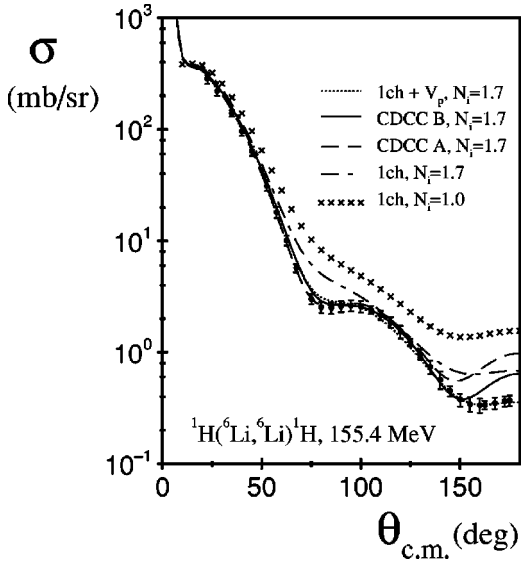

FIG. 2. Results of calculations for the elastic scattering of ^{6}Li from ^{1}H. The experimental data are from Ref. [22]. See text for details.

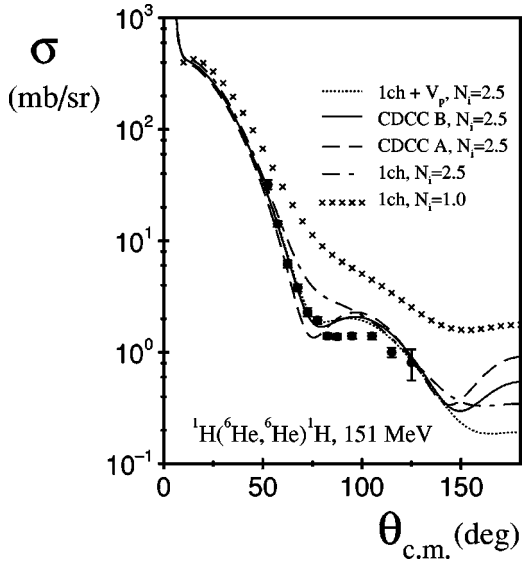

FIG. 3. Same as Fig. 2 but for the elastic scattering of ^{6}He from ^{1}H. In the calculations set II of the $\alpha+2n$ binding potential parameters was used. The experimental data are from Wolski *et al.* [2].

CDCC calculations, shown by the dashed curve in Fig. 2, were performed with the wave functions representing energy bins of the ^{6}Li continuum normalized to unity. Such a procedure changes the amplitude of the wave function for small separation between the α-d clusters. To establish how large the effect of this normalization can be, similar CDCC calculations but with non-normalized continuum wave functions were performed. Results of these calculations are shown by the solid curve in Fig. 2 (CDCC *B*). They are closer to the experimental data at backward angles. The results do not depend on the upper limit of the integration radius provided that it is larger than 30 fm. In these calculations some strength of the coupling to the continuum is missing, but it is not artificially shifted to the small α-d separations like in the CDCC *A* calculations. We believe that the calculations with non-normalized wave functions of the continuum give more realistic results.

In summary, a good description of the ^{6}Li$+^1$H elastic scattering experimental data over a wide range of angles has been obtained, with the central and coupling potentials calculated from optical model interactions for $p+^4$He and $d+^1$H found from fitting the corresponding experimental data. However, the imaginary part of the second input potential had to be renormalized by a factor $N_i=1.7$. This larger imaginary part can account for effects that are not included in the coupling scheme; for example, one-neutron transfer reaction or direct breakup via states in the continuum located above the excitation energy of about 9.5 MeV, the upper limit in the CDCC calculations.

C. Elastic and inelastic scattering results

Calculations similar to those carried out for ^{6}Li were performed for ^{6}He$+^1$H scattering. The results of these calculations with the potentials derived from the $p+^4$He and $d+^1$H optical model potentials, listed in Table 2, by means of the single-folding method overpredict the cross-section data obtained experimentally, as was the case for ^{6}Li. When the imaginary part of the input $d+^1$H potential was renormalized by $N_i=2.5$, the calculated results became much closer to the data as shown by the dashed curve in Fig. 3. This increase of the renormalization factor could be caused by a difference between the breakup of the deuteron and the breakup of the dineutron within the ^{6}He continuum.

As a next step, full CDCC calculations with wave functions of the continuum (CDCC *A* in Fig. 3) normalized to unity and without this normalization (CDCC *B*) were performed. There are no data available for scattering angles larger than 125° where the effect of normalization is the largest, but the change in calculated results is very similar to that seen for the ^{6}Li$+^1$H scattering system. Calculations with non-normalized continuum wave functions generate lower cross sections at backward angles.

The nuclei ^{6}He and ^{6}Li have much in common—they are very loosely bound, they have similar rms matter radii, and they do not have any bound excited states. The breakup threshold for ^{6}Li into an α particle and a deuteron is one-half an MeV higher than that for ^{6}He$\rightarrow\alpha+2n$. It was found by Keeley and Rusek that the difference in the α-breakup thresholds enhances the ^{6}Li$\rightarrow\alpha+d$ breakup cross section over that of ^{7}Li$\rightarrow\alpha+t$ [23]. One may surmise then that the so-called polarization potential V_p, which simulates in one-channel calculations effects of channel couplings, should be stronger for ^{6}He than for ^{6}Li as was demonstrated for ^{6}Li and ^{7}Li. Polarization potentials for both scattering systems have been extracted from the CDCC *B* calculations using the method of Thompson *et al.* [24]. Their dependence on the separation between the colliding nuclei is shown in Fig. 4. At the region important for scattering (around 4 fm), their imaginary parts are very similar while the real parts differ—the potential for ^{6}He is stronger than the potential for ^{6}Li. The real potential for ^{6}He is repulsive, as is the potential for

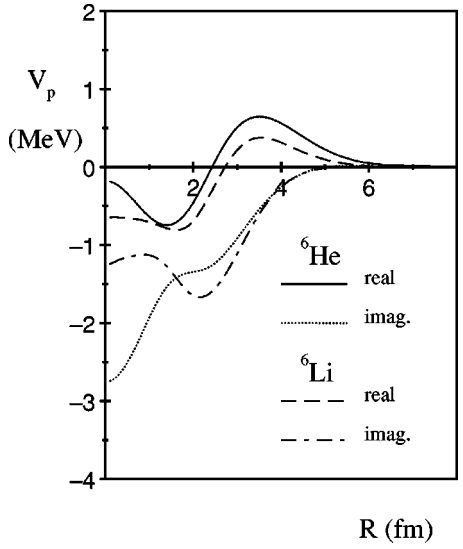

FIG. 4. Polarization potentials deduced from CDCC *B* analyses of ^{6}Li and ^{6}He scattering from ^{1}H.

^{6}Li and other loosely bound nuclei. At the projectile-target separation of 4 fm its strength is about 25% of the *bare* single-folding potential. This result is in agreement with the recent work of Gupta *et al.* [11] who found that to reproduce ^{6}He$+^1$H elastic scattering data at 151 MeV by optical model calculations with the real potential derived from a nucleon-nucleon interaction, the depth of the potential had to be reduced by about 30%.

To check how well the one-channel calculations with the central potential of the form

$$U_{p\text{-}^6\mathrm{He}}(R)=U^{SF}_{p\text{-}^6\mathrm{He}}(R)+V_p(R), \tag{3}$$

where $U^{SF}_{p\text{-}^6\mathrm{He}}(R)$ is the *bare* single-folding potential, simulate the results of full CDCC *B* calculations, such calculations were performed for both scattering systems. The results are presented by dotted curves in Figs. 2 and 3. They are very close to the results obtained using the CDCC *B* method apart from the backward angles. Surprisingly, for the ^{6}Li $+^1$H scattering, one-channel calculations with the polarization potential included fit the experimental data better at backward scattering angles than do the original CDCC *B* calculations.

CDCC *B* calculations were performed with three different geometries for the $\alpha+2n$ binding potentials, sets I, II, and III of Table I. Each set corresponds, among others, to the different value of the reduced transition probability $B(E2;\mathrm{g.s.}\rightarrow 2^+)$ between the ground state and the resonant state of ^{6}He.

The results of the CDCC *B* calculations for ^{6}He$+^1$H elastic scattering are shown in Fig. 5. As expected, the calculations with potential set III, giving the weakest coupling, generated the largest values of the elastic scattering cross sections while the calculations with set I gave the smallest values.

For the inelastic scattering exciting ^{6}He to its 2^+ resonant state, the situation is opposite—CDCC *B* calculations, corresponding to the largest value of the reduced transition probability, gave the largest values of the differential cross section, as shown in Fig. 6. Future experimental data for this process will serve as a stringent test of the present calculations.

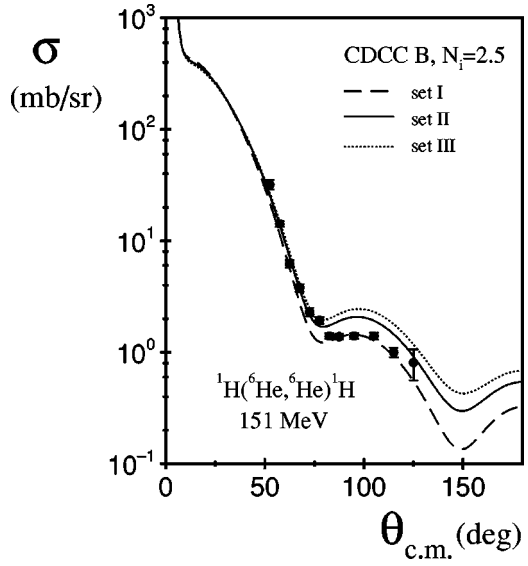

FIG. 5. Results of CDCC calculations for ^{6}He$+^1$H elastic scattering with the three different sets of $\alpha+2n$ binding potentials listed in Table I. The experimental data are from Ref. [2].

The CDCC *B* calculations have been repeated at the higher incident energy of 250 MeV without any change in input parameters. Experimental data for ^{6}He$+^1$H elastic scattering for this energy were published earlier by Cortina-Gil *et al.* [25]. There is also another set of data, published very recently [26], measured at the slightly lower energy of

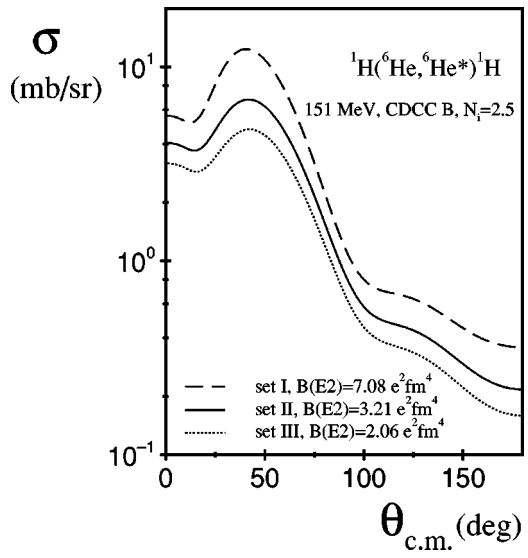

FIG. 6. Same as Fig. 5 but for the inelastic scattering of ^{6}He from ^{1}H, leading to the 2^+ resonance of the projectile at excitation energy of 1.8 MeV.

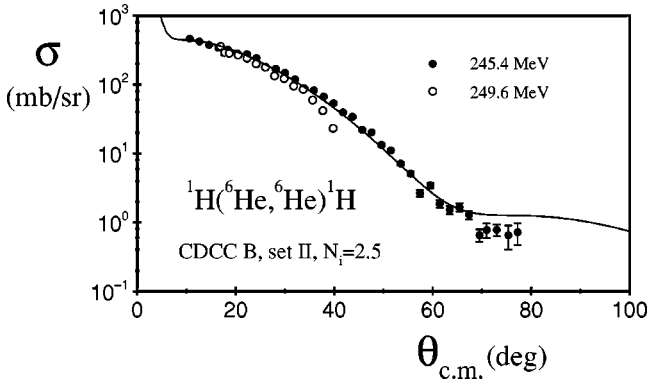

FIG. 7. Results of the CDCC *B* calculations for the incident energy of 250 MeV of the ^{6}He beam. The data sets at 245.4 MeV and 249.6 MeV are from de Vismes *et al.* [26] and Cortina-Gil *et al.* [25].

245 MeV. The results of the calculations are plotted in Fig. 7 together with the two sets of data.

III. TRANSFER REACTION

A. Exit-channel potential

In order to calculate the cross section for the ^{1}H(^{6}He,α)^{3}H transfer reaction at the incident energy of 151 MeV, the optical model potential for $\alpha+^3$H elastic scattering at the corresponding energy of 67.9 MeV is needed. To our knowledge this scattering has not been investigated experimentally at this energy, but there are data for a similar system, $\alpha+^3$He, at a wide range of energies [27,28]. It is also well known that the process of one-neutron transfer, not distinguishable experimentally from the elastic scattering, contributes significantly to the final results [29]. This fact makes the analysis of α elastic scattering from ^{3}He very difficult. On the other hand, results of calculations for the ^{1}H(^{6}He,α)^{3}H reaction strongly depend on the interaction in the exit channel, therefore calculations with three different $\alpha+^3$He optical model potentials have been performed. The parameters of the potentials are listed in Table II.

The potential *A* was obtained by Vincent and Boschitz [30] from an optical model analysis of $\alpha+^3$He elastic scattering at 42 MeV. It reproduces the angular distribution of the differential cross section very well at this energy, but its description of the data measured at the higher energy of 65.3 MeV, much closer to that required, is rather poor. Since this potential was used in all previous analyses of the ^{1}H(^{6}He,α)^{3}H reaction [2,4,5], it was also used in this work for comparison.

The parameters of potential *A* were used as starting values for a parameter search carried out to improve the description of the experimental data for the elastic scattering of α particles from ^{3}He at 65.3 MeV. Optical potential *B* resulted from this search. Although the fit is still far from perfect, it reproduces the gross features of the measured angular distribution.

Neudatchin *et al.* [29] studied the α-*t* scattering system more microscopically and derived an *L*-dependent potential that describes the phase shifts for this system over a wide energy range. A simplified *L*-independent form of this potential was also applied to the analysis of the ^{1}H(^{6}He,α)^{3}H transfer reaction (potential *C*).

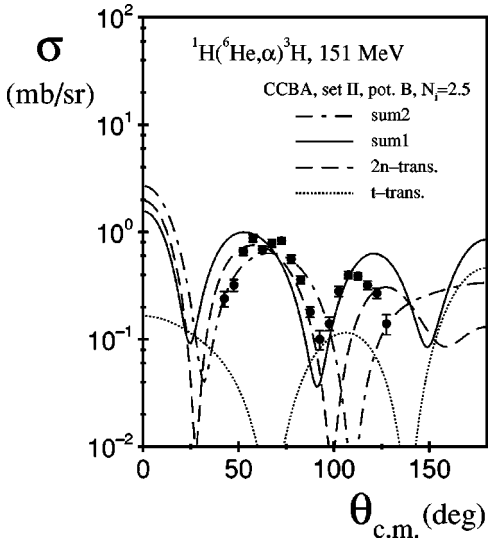

FIG. 8. Results of the CCBA calculations for the transfer reaction. The dot-dashed and solid curves correspond to the different signs of the ^{6}He$=t+t$ spectroscopic amplitude. The data set is from Wolski *et al.* [2].

B. CCBA calculations

Before starting full CCBA calculations several tests were performed using the simple DWBA method. In the DWBA, the transition matrix element for dineutron stripping from ^{6}He to ^{1}H can be written either in *post* or *prior* form:

$$T_{post}=\langle \chi_{\alpha,t} \quad \Psi_t|U_{\alpha\text{-}p}+U_{\alpha\text{-}2n}-U_{\alpha\text{-}t}|\Psi_{^6\mathrm{He}} \quad \chi_{p,^6\mathrm{He}}\rangle, \tag{4}$$

$$T_{prior}=\langle \chi_{p,^6\mathrm{He}} \quad \Psi_{^6\mathrm{He}}|U_{\alpha\text{-}p}+U_{p\text{-}2n}-U^{SF}_{p\text{-}^6\mathrm{He}}|\Psi_t \quad \chi_{\alpha,t}\rangle, \tag{5}$$

where χ_i are the scattering wave functions in the entrance and exit channels, Ψ_i are the bound-state wave functions of the triton, and ^{6}He, U_i are the interactions for the different systems listed in Tables I and II and, for p-^{6}He, generated by single-folding calculations. This test showed that the final results of the calculations corresponding to both forms are very close. The CCBA calculations were performed using the *post* form.

The results of the CCBA calculations are shown in Fig. 8 with potential *B* in the exit channel for the dineutron-transfer reaction (dashed curve). In the calculations couplings to the unbound states of ^{6}He as well as transfer of the dineutron from those states were included. The wave functions representing continuum bins were not normalized to unity as in the CDCC *B* calculations. The parameters of the Woods-Saxon potential that binds the transferred dineutron to the proton to form the triton were taken from Ref. [31] while the spectroscopic amplitude for this projection was adopted from calculations of Nemets *et al.* [8]. The results of the CCBA calculations reproduced the forward angle oscillation of the

differential cross section quite well while at scattering angles larger than 100° there is a shift between the data and the calculations.

Despite the fact, that the $^6\mathrm{He}\rightarrow t+t$ breakup threshold is well above the threshold for $^6\mathrm{He}\rightarrow \alpha+2n$, the ground-state wave function of ^{6}He has a significant component originating from $t+t$ clustering. Studies by Clarke [6] based on *t*-transfer reactions induced by tritons on a number of target nuclei supported a theoretical prediction for the $^6\mathrm{He}=t+t$ spectroscopic amplitude to be equal to -1.33 [8]. This value was also used by Timofeyuk and Thompson [9] in their analysis of the $^6\mathrm{He}(p,\alpha)^3\mathrm{H}$ transfer reaction. In the present CCBA calculations the *t* transfer in the coupling scheme is included to find out if its presence can reduce the shift between the data and the calculations at backward angles. In test calculations, it was found that the final results depend only weakly on the parameters of the potential binding the two tritons in ^{6}He. Therefore the same parameters for this potential, as used by Timofeyuk and Thompson [9], were used (Table I). Calculations with the spectroscopic amplitude for $t+t$ clustering equal to -1.33 changed the results mostly at backward angles, as expected, but generated too large a cross section value, so the magnitude of this amplitude was varied in order to obtain the best possible description of the experimental data. The dotted curve in Fig. 8 shows the contribution to the $^1\mathrm{H}(^6\mathrm{He},\alpha)^3\mathrm{H}$ differential cross section due to triton transfer with the $t+t$ spectroscopic amplitude reduced to -0.5. The coherent sum of the two processes, transfer of a dineutron and a triton, is shown in Fig. 8 by the solid curve. Addition of the *t*-transfer component produced better agreement with the experimental data. The final result was found to be very sensitive to the sign of the $t+t$ spectroscopic amplitude. The dot-dashed curve shows results when the sign of the $^6\mathrm{He}=t+t$ amplitude was reversed.

The results of the CCBA calculations for the $^1\mathrm{H}(^6\mathrm{He},\alpha)^3\mathrm{H}$ reaction depend much less on the different $\alpha+2n$ binding potentials than the elastic or inelastic scattering. They strongly depend, however, on the choice of the optical potential in the exit channel. The results of CCBA calculations with the α-*t* potentials from Table II are shown in Fig. 9. All three calculations are the coherent sums of the dineutron and triton transfer processes with the $t+t$ spectroscopic amplitude equal to -0.5. The best description of the experimental data was obtained with potential *A*, used in all previous analyses of this data set. Calculations with the microscopic potential of Neudatchin *et al* [29] generated the worst result.

One of the aims of the present work was to study the role of the dineutron transfer from $^6\mathrm{He}\rightarrow\alpha+2n$ breakup states. In Fig. 10 we compare angular distributions of the differential cross section for the $^1\mathrm{H}(^6\mathrm{He},\alpha)^3\mathrm{H}$ transfer reaction calculated by means of the CCBA method with the simple DWBA calculations. In the calculations, potential *B* of Table I was used in the exit channel. In the DWBA 1 calculation, shown by the dashed curve, the couplings to the ^{6}He unbound states were not included as the potential $U_{p\text{-}^6\mathrm{He}}(R)$ in the entrance channel was a central single-folding potential $U^{SF}_{p\text{-}^6\mathrm{He}}(R)$ generated from $p+^4$He and $d+^1$H potentials. In

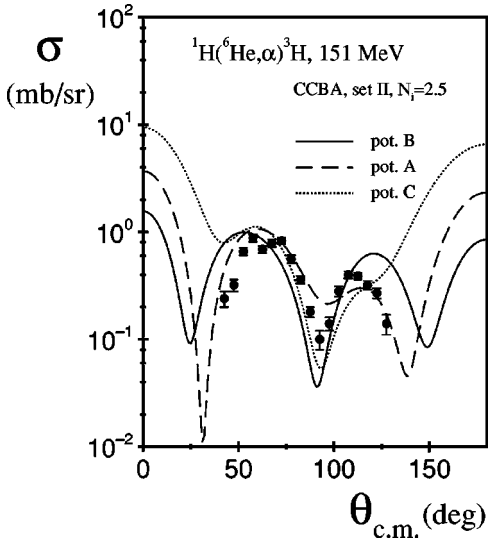

FIG. 9. Dependence of the results of the CCBA calculations on the choice of the $\alpha+^3$H optical model potential. The potential parameters are listed in Table I.

the DWBA 2 calculation, $U_{p\text{-}^6\mathrm{He}}(R)=U^{SF}_{p\text{-}^6\mathrm{He}}(R)+V_p$ (R), so the couplings to the unbound states are in some sense included but not the dineutron transfer from those states. Both DWBA calculations gave rather similar results suggesting that the influence of the couplings to the ^{6}He breakup channels is small. They differ from the results of the CCBA calculation mainly at forward scattering angles, which reflects the role played by the transfer of the dineutron from the unbound states of ^{6}He. This role is reduced by the *t*-transfer contribution that adds coherently to the contribution of the dineutron transfer.

The CCBA calculations were repeated at the higher incident energy of 250 MeV in order to see how the results depend on the energy of the ^{6}He beam. All the input param-

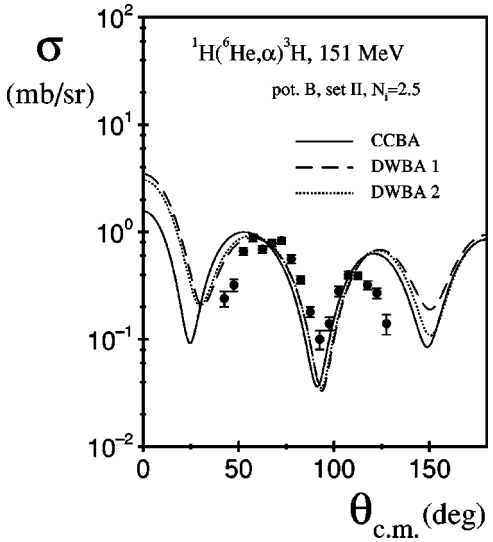

FIG. 10. Comparison of the results of CCBA calculations with the results of DWBA calculations with (DWBA 2) and without (DWBA 1) the polarization potential in the entrance channel.

TABLE III. Calculated cross sections for interaction of ^{6}He with protons at the two incident energies.

E_{lab} (MeV)	Total reaction (mb)	Total breakup (mb)	Breakup via 2^+ resonance (mb)	$(^6\mathrm{He},\alpha)$ transfer (mb)
151	492.2	116.0	27.8	5.6
250	402.2	88.4	21.6	1.4

eters were the same as those at 151 MeV. The results are listed in Table III. Generally, the calculated total cross sections for different processes decrease with energy. The most dramatic reduction is observed for the transfer reaction. It is interesting to note that the calculated value of the total reaction cross section at 250 MeV is very close to that measured by de Vismes *et al.* [26] at the slightly lower energy of 245 MeV.

IV. CONCLUSIONS

A consistent analysis of existing $^6\mathrm{He}+^1\mathrm{H}$ scattering data at 151 MeV as well as the $^1\mathrm{H}(^6\mathrm{He},\alpha)^3\mathrm{H}$ transfer reaction has been performed by means of the coupled channels method. The present analysis uses a simple two-body cluster model of ^{6}He. Only two *free* parameters were used—the depth of the imaginary part of the input $d+^1\mathrm{H}$ optical potential and the spectroscopic amplitude for $t+t$ clustering in the ^{6}He ground state. All other parameters were fixed by previous studies.

In order to obtain a reasonable description of the elastic scattering data the depth of the imaginary part of the $d+^1\mathrm{H}$ potential used in the calculations had to be renormalized by a factor of $N_i=2.5$. This can be due to the limited number of processes explicitly included in the coupling scheme. For example, the one-neutron transfer reaction was not included in the analysis. The present analysis shows that the elastic scattering of ^{6}He by a proton target is influenced by breakup of the projectile into an α particle and two neutrons. This breakup can be simulated in simple optical model calculations by a complex polarization potential added to the central *bare* potential. This induced polarization potential exhibits similar properties to those found for other loosely bound projectiles: its real part is repulsive at projectile-target separations important for the scattering and its strength is about 25% of the single-folding potential. This result is in agreement with the value reported by Gupta *et al.* [11]. The polarization potential for ^{6}He is more repulsive than that for ^{6}Li, which reflects the different binding energies of the two nuclei.

In this work predictions for the differential cross section of $^6\mathrm{He}+^1\mathrm{H}$ inelastic scattering to its resonant 2^+ state at an excitation energy of 1.80 MeV were made. New experimental data for this process will test these results.

Large coherent effects due to contributions coming from two-neutron and *t* transfer, processes that are experimentally indistinguishable, were found for the $^1\mathrm{H}(^6\mathrm{He},\alpha)^3\mathrm{H}$ transfer reaction. These effects can make the study of detailed $\alpha+2n$ configurations in the ^{6}He ground state very difficult. The transfer reaction was affected by the breakup of the projectile mainly at forward scattering angles.

The present analysis did not give a conclusive value for the $^6\mathrm{He}_{\mathrm{g.s.}}=t+t$ spectroscopic amplitude as the results of the calculations are strongly dependent on the poorly known $\alpha+t$ interaction. However, calculations performed with three different interactions lead to a similar conclusion—the value of the spectroscopic amplitude for $^6\mathrm{He}_{\mathrm{g.s.}}=t+t$ clustering was found to be much smaller than predicted by two-body shell model calculations [8]. This value is very close to that suggested by Wolski *et al.* [2] and only slightly smaller than the value calculated by Arai *et al.* [7] from a four-cluster model of $^6\mathrm{He}_{\mathrm{g.s.}}$. In this model the α cluster being the core particle is described as a three-nucleon cluster and a single nucleon. The calculations were quite sensitive to the relative sign of the $^6\mathrm{He}_{\mathrm{g.s.}}=\alpha+$dineutron and $^6\mathrm{He}_{\mathrm{g.s.}}=t+t$ spectroscopic amplitudes, with the sign found in the present analysis agreeing with theoretical predictions.

ACKNOWLEDGMENTS

This work was financially supported by the National Atomic Energy Agency of Poland, a PST.CLG 974757 NATO grant, and the U.S. National Science Foundation.

[1] G.M. Ter-Akopian, A.M. Rodin, A.S. Fomichev, S.I. Sidoruk, S.V. Stepantsov, R. Wolski, M.L. Chelnokov, V.A. Gorshkov, A.Yu. Lavrentev, V.I. Zagrebaev, and Yu.Ts. Oganessian, Phys. Lett. B **426**, 251 (1999).

[2] R. Wolski, A.S. Fomichev, A.M. Rodin, S.I. Sidoruk, S.V. Stepantsov, G.M. Ter-Akopian, M.L. Chelnokov, V.A. Gorshkov, A.Yu. Lavrentev, Yu.Ts. Oganessian, P. Roussel-Chomaz, W. Mittig, and I. David, Phys. Lett. B **467**, 8 (1999).

[3] M.V. Zhukov, B.V. Danilin, D.V. Fedorov, J.M. Bang, I.J. Thompson, and J.S. Vaagen, Phys. Rep. **231**, 151 (1993).

[4] Yu.Ts. Oganessian, V.I. Zagrebaev, and J.S. Vaagen, Phys. Rev. C **60**, 044605 (1999).

[5] Yu.Ts. Oganessian, V.I. Zagrebaev, and J.S. Vaagen, Phys. Rev. Lett. **82**, 4996 (1999).

[6] N.M. Clarke, J. Phys. G **18**, 917 (1992).

[7] K. Arai, Y. Suzuki, and R.G. Lovas, Phys. Rev. C **59**, 1432 (1999).

[8] O.F. Nemets, V.G. Neudatchin, A.T. Rudchik, Yu.F. Smirnov, and Yu.M. Tchuvil'skii, *Nucleon Clusters in Atomic Nuclei and Many-Nucleon Transfer Reactions* [in Russian] (Ukrainian

Academy of Science, Institute for Nuclear Research, Kiev, 1988).
[9] N.K. Timofeyuk and I.J. Thompson, Phys. Rev. C **61**, 044608 (2000).
[10] K. Rusek and K.W. Kemper, Phys. Rev. C **61**, 034608 (2000).
[11] D. Gupta, C. Samanta, and R. Kanungo, Nucl. Phys. **A674**, 77 (2000).
[12] I.J. Thompson, Comput. Phys. Rep. **7**, 167 (1988).
[13] Y. Sakuragi, M. Yahiro, and M. Kamimura, Prog. Theor. Phys. Suppl. **89**, 136 (1986).
[14] Yu.M. Tchuvil'skii and Yu.F. Smirnov, Phys. Rev. C **15**, 84 (1977).
[15] A.T. Rudchik and Yu.M. Tchuvil'skii, Ukr. Phys. J. **30**, 819 (1985).
[16] T. Aumann, D. Aleksandrov, L. Axelsson, T. Baumann, M.J. Borge, L.V. Chulkov, J. Cub, W. Dostal, B. Eberlein, Th.W. Elze, H. Emling, H. Geissel, V.Z. Goldberg, M. Glovkov, A. Grünschloss, M. Hellström, K. Hencken, J. Holeczek, R. Holzmann, B. Jonson, A.A. Korshenninikov, J.V. Kratz, G. Kraus, R. Kulessa, Y. Leifels, A. Leistenschneider, T. Leth, I. Mukha, G. Münzenberg, F. Nickel, T. Nilsson, G. Nyman, B. Petersen, M. Pfüzner, A. Richter, K. Riisager, C. Scheidenberger, G. Schrieder, W. Schwab, H. Simon, M.H. Smedberg, M. Steiner, J. Stroth, A. Surowiec, T. Suzuki, O. Tengblad, and M.V. Zhukov, Phys. Rev. C **59**, 1252 (1999).
[17] K. Rusek, P.V. Green, P.L. Kerr, and K.W. Kemper, Phys. Rev. C **56**, 1895 (1997).
[18] F. Hinterberger, G. Mairle, U. Schmidt-Rohr, and G.J. Wagner, Nucl. Phys. **A111**, 265 (1968).
[19] D.J. Plummer, K. Ramavataram, T.A. Hodges, D.G. Montague, A. Zucker, and N.K. Ganguly, Nucl. Phys. **A174**, 193 (1971).
[20] J. Raynal, code ECIS79 (unpublished).
[21] G.E. Thompson, M.B. Epstein, and T. Sawada, Nucl. Phys. **A142**, 571 (1970).
[22] K.H. Bray, M. Jain, K.S. Jayaraman, G. Lobianco, G.A. Moss, W.T.H. Van Oers, and D.O. Wells, Nucl. Phys. **A189**, 35 (1972).
[23] N. Keeley and K. Rusek, Phys. Lett. B **427**, 1 (1998).
[24] I.J. Thompson, M.A. Nagarajan, J.S. Lilley, and M.J. Smithson, Nucl. Phys. A **505**, 84 (1989).
[25] M.-D. Cortina-Gil, P. Roussel-Chomaz, N. Alamanos, J. Barrette, W. Mittig, F.S. Dietrich, F. Auger, Y. Blumenfeld, J.M. Casandjian, M. Chartier, V. Fekou-Youmbi, B. Fernandez, N. Frascaria, A. Gillibert, H. Laurent, A. Lepine-Szily, N.A. Orr, J.A. Scarpaci, J.L. Sida, and T. Suomijarvi, Phys. Lett. B **401**, 9 (1997).
[26] A. de Vismes, P. Roussel-Chomaz, W. Mittig, A. Pakou, N. Alamanos, F. Auger, J.-C. Angélique, J. Barrette, A.V. Belozyorov, C. Borcea, W.N. Catford, M.-D. Cortina-Gil, Z. Dlouhy, A. Gillibert, V. Lapoux, A. Lepine-Szily, S.M. Lukyanov, F. Marie, A. Musumarra, F. de Oliveira, N.A. Orr, S. Ottini-Hustache, Y.E. Penionzhkevich, F. Sarazin, H. Savajols, and N. Skobelev, Phys. Lett. B **505**, 15 (2001).
[27] W. Fetscher, E. Seibt, and Ch. Weddigen, Nucl. Phys. **A216**, 47 (1973).
[28] P. Schwandt, B.W. Ridley, S. Hayakawa, L. Put, and J.J. Kraushaar, Phys. Lett. **30B**, 30 (1969).
[29] V.G. Neudatchin, V.I. Kukulin, A.N. Boyarkina, and V.P. Korennoy, Lett. Nuov. Cim. **5**, 834 (1972).
[30] J.S. Vincent and E.T. Boschitz, Nucl. Phys. **A143**, 121 (1970).
[31] M.F. Werby, M.B. Greenfield, K.W. Kemper, D.L. McShan, and S. Edwards, Phys. Rev. C **8**, 106 (1973).